ChemElectroChem

Research Article
doi.org/10.1002/celc.202201032

Chemistry Europe
European Chemical Societies Publishing

www.chemelectrochem.org

Mass Transport Influence in the SO_2 Oxidation Reaction on Au Electrodes

Leonardo D. De Angelis,[b] Susana I. Córdoba de Torresi,[b] and André H. B. Dourado*[a]

The use of fossil fuels as energy source is unsustainable in the long term and net-zero carbon processes need to be implemented to maintain environmental balance. One could make use of assisted water electrolysis to produce clean hydrogen and avoid high overpotentials observed for the oxygen evolution reaction by switching to the SO_2 oxidation reaction (SO_2OR). This process exhibits a complex mechanism on Au electrodes, which is strongly affected by convection, exhibiting an anti-Levich behavior, in which the limiting current linearly decreases with the square root of the rotation rate. Likewise, the bi-stability region observed in the *j*/*E* profiles narrows in a sigmoidal profile with the rotation rate, leading to a non-linear phenomenon with two controlling parameters, mass transport and potential applied. These events were understood to be related to the changing in the reaction mechanism by controlling the electrode rotation, much related to the decrease in the current aforementioned.

Introduction

The increasing use of fossil fuels over the last decades to fulfill the growth of energy demand[1] was followed by global atmospheric pollution and environmental problems, such as the climate change.[2] These matters promoted the search for renewable energy sources, such as photovoltaic and wind power, along with the development of energy storage technologies. One of the most promising options is to storage this energy in the form of chemical bonds through the synthesis of solar fuels.[3–5] H_2 is an example of such molecule, a gas capable to release up to four times more energy than fossil fuels when converted to water.[6]

H_2 is a scarce component in the atmosphere and needs to be synthesized. The main electrochemical process for its generation is water electrolysis. Despite being a widely investigated reaction,[7–9] this process is constrained by the high energy needed for the oxidative reaction, the oxygen evolution reaction (OER, $E^\circ = 1.23\ V_{SHE}$).[10] Besides, there are also kinetic limitations that increase the operational potential up to more than 1.80 V_{RHE}, limiting its applicability. These factors guided the search for new materials and alternative anodic reactions for water electrolysis,[10–13] in a process called assisted water electrolysis.[14,15] A possible substitute reaction to avoid OER limitations is the SO_2 oxidation reaction (SO_2OR, $E^\circ = 0.16\ V_{SHE}$) to sulfuric acid. SO_2 is a pollutant with a harmful dose of solely 5 ppm[16] and is generated during fossil fuels combustion due to the burning of sulfurous contaminants present in these energy sources.[17] The use of SO_2 in assisted water electrolysis is a way to produce clean H_2 with lower energy inputs, while consuming an environmental pollutant.

SO_2OR has been studied for the last years[18–26] and authors generally differ about the intermediates formed, although the proposition of catalytic poisonous species is a convergence point. Recent studies published by our group propose mechanisms to the SO_2OR on polycrystalline Au (Scheme 1).[24–26] It was shown that the reaction presents high dependence on both electrode and supporting electrolyte employed.

Two distinct SO_2 adsorption conformations can be noted in Scheme 1, one being by the sulfur atom (Au-SO_2) and the other by the oxygen atoms (SO_2-Au). The preferential adsorption

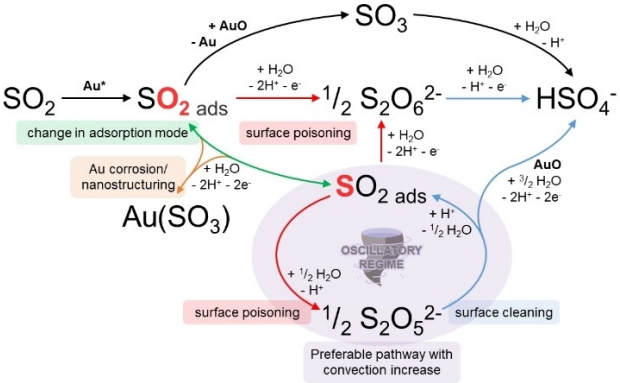

Scheme 1. Proposed mechanism for the SO_2OR on Au. Sulfur and oxygen atoms are highlighted in red to represent two distinct adsorption modes. The change in adsorption mode is highlighted in green. Poisoning steps are highlighted in red. Cleaning steps are highlighted in blue. Oscillatory mechanism is emphasized in purple. Au* represents a free adsorption site.

[a] *Dr. A. H. B. Dourado*
Departamento de Físico-Química
Instituto de Química de São Carlos, Universidade de São Paulo
Av. Trab. São Carlense, 400, 13566-590, São Carlos, SP, Brazil
E-mail: andre.dourado@usp.br
dourado@iq.usp.br
[b] *L. D. De Angelis, Prof. Dr. S. I. Córdoba de Torresi*
Departamento de Química Fundamental
Instituto de Química, Universidade de São Paulo
Av. Prof. Lineu Prestes, 748, 05508-000, São Paulo, SP, Brazil

Supporting information for this article is available on the WWW under https://doi.org/10.1002/celc.202201032

mode is dependent of the electrolyte chaotropicity, which determines if the conditions either favor the generation of dithionate ($S_2O_6^{2-}$) or enter oscillatory regime (pathways emphasized in purple in Scheme 1) with pyrosulfite ($S_2O_5^{2-}$). In these previous[24–26] and in the present work, electrolytes were chosen to mimic the Hofmeister series,[27,28] going from a chaotropic (solution containing only $HClO_4$ as supporting electrolyte), to a kosmotropic media (containing just H_2SO_4). In chaotropic media, the Au-SO_2 adsorption mode is favored and thus an oxidation-regeneration cycle with $S_2O_5^{2-}$ occurs, giving rise to oscillations. This oscillator is classified as hidden negative differential resistance (HNDR)[24,25] and explains why these oscillations are present under potentiostatic and galvanostatic regimes.

Even in a deep discussion about the SO_2OR mechanism, there is not much information regarding the mass transport role in this process and how it may affect the oscillatory regime onto Au electrodes. It was shown that Au presents a strong interaction with sulfur species[29] and higher catalytic activity when compared to other electrodes.[30] This work aims at performing experiments in reported oscillating conditions[24–26] (SO_2-saturated solutions), utilizing potential perturbations techniques and electrochemical impedance spectroscopy (EIS) for elucidating factors that influence on the SO_2OR.

Results and Discussion

The SO_2OR on Au electrodes have already been reported as a complex electrochemical reaction and presents non-linear dynamics related to poisoning-cleaning cycles.[24–26] It is very common to find that non-linear phenomena in chemical reactions are easily affected by diffusion.[31–35] Thus, the first step to analyze the convection influence on the SO_2OR was to perform triangular potential perturbations at different rotation rates in different electrolytes. It is presented in Figure 1 the *j*/*E* profiles obtained for a 50% H_2SO_4, $HClO_4$ electrolyte mixture.

The j/E profiles in Figure 1 present a typical shape for SO_2OR on Au,[24–26] which consists of an increment in the anodic current until a plateau, during the forward scan. After that, current drops to zero at a given descending potential (E_d), indicating that the electrode is covered by insulating compounds, i.e., poisoned. During the back scan, current sharply increases to another plateau at a given ascending potential (E_a), indicating that a cleaning process is taking place. This reaction is always at potentials more negative than E_d. The potential window between these two is referred to as bi-stability region. These behaviors can also be seen for other electrolytes (Figure S1).

The shape of the j/E profiles in Figure 1 let clear that E_d and E_a are two saddle-node bifurcations,[36] as it can be noticed that the bi-stability region narrowed with the rotation increment. However, this narrowing is not due to E_d being shifted to more negative potentials while E_a is for more positive ones, in fact, both shift to more negative potentials with the rotation increment. For further investigation of this phenomenon, the codimension two-bifurcation diagram of E_d and E_a with the rotation rate, for three different electrolytes, is displayed in Figure 2.

In Figure 2, despite both E_d and E_a being affected by diffusion, the E_d sigmoidal drop to more negative potentials is more pronounced. At low rotation rates, E_d is more positive for lower H_2SO_4 content. For all employed electrolytes, 1.5 V_{RHE} was observed as most negative E_d. As for the E_a saddle-node, a drop in potential is indeed noticeable, especially in the presence of $HClO_4$; however, this behavior is not as expressive as for E_d. In case of the existence of a cusp co-dimension two-bifurcation, both saddle-nodes would merge, which should be expected to occur at high rotation rates, which is not observed. This could be due to experimental limitations as turbulent flow is observed at rotation rates higher than 2500 rpm. Nevertheless, electron transfer processes are already known to be related to cusp bifurcations,[37] but not much is presented in the literature

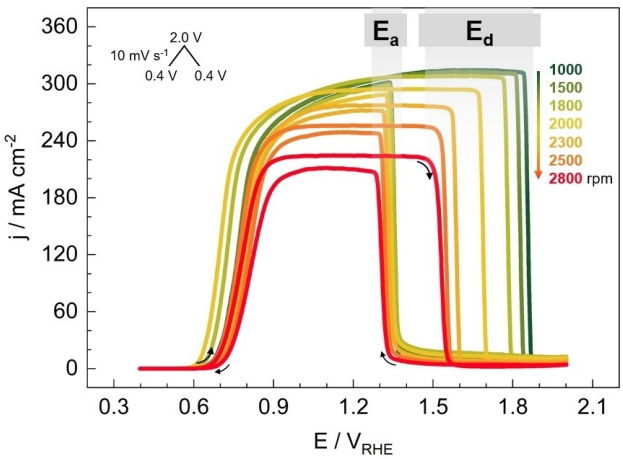

Figure 1. *j*/E profiles obtained for SO_2OR on Au in the 50% H_2SO_4, $HClO_4$ electrolyte. Black curved arrows indicate the potential scan direction. E_d and E_a indicate the descending and ascending potential region with rotation increment, respectively. Colored notes and arrow indicate the rotation increment direction.

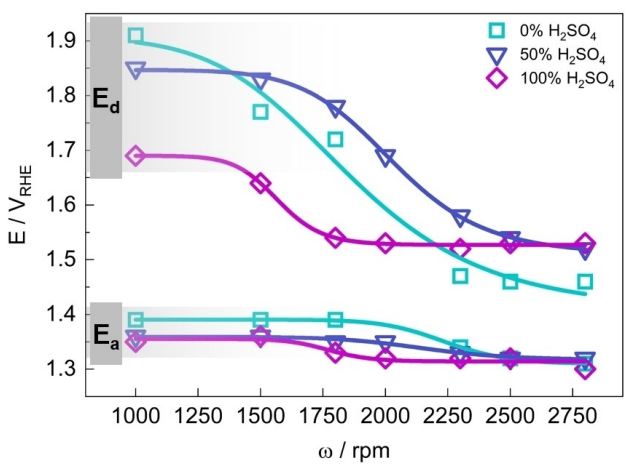

Figure 2. Co-dimension two-bifurcation diagram, in which both saddle-node bifurcations (E_d and E_a) observed for the j/E profiles in Figure 1 are plotted against the rotation rate. Symbols represent the experimental data and solid lines are only intended as a visual guide.

about the influence of mass transport in such behavior. Therefore, it is interesting to highlight that diffusion can also play an important role on this phenomenon. Nevertheless, the absence of a clear cusp catastrophe can be related to the fact that the proper plane for its representation was not found, since it is in the definition of the property that the fix points diagram folds on itself.

The sigmoidal shape for the E_d observed in Figure 2 is very similar to the proposed in the literature for electrochemical-chemical-electrochemical (ECE) mechanisms but considering the current response to rotation variation.[38–40] In that model, a higher number of electrons is observed at lower rotations than at higher. This denotes that some desorbed intermediate is generated by a first electrochemical step, consumed by a chemical reaction, and then it is finally consumed in a last electrochemical step. At high rotation rates, this desorbed intermediate is pushed away from the electrode by convection faster than the chemical step. In this way, the final electrochemical step is not observed and the number of electrons at high rotations is decreased.[38,39,41] Following this logic, one can argue that the bi-stability narrowing in Figure 2 might also signify a change in the observed reaction pathway by controlling the convection. The main problem with this logic is that potential and number of electrons are inversely proportional, by the Nernst equation, so a decrease in the number of electrons should be related to a shift to more positive potentials. In this way, what would better explain the shift to more negative potentials is that the first electrochemical step needs lower overpotentials to be observed, while the second has higher activation barriers. The increment in rotation rate made the rate determining step (RDS) observed to be different. In other experiments (Figure S2), it was observed that potential oscillations are observed when the electrode is rotated at higher rates, which may indicate that the pyrosulfite pathway formation (Scheme 1) is indeed being favored by convection. This change in mechanism path corroborates the differences in RDS proposed by Figure 2 interpretation.

In Figure 1 the current is not following the pattern expected for regular RDE experiments, as Levich or Koutécky-Levich models, based on the Fick's diffusion laws.[42–44] In these models, the current is directly proportional to the square root of rotation rate. This behavior is the opposite of what is observed in the present case, suggesting that the steps that are most affected by the mass transport are generation of catalytic poison. To further investigate this matter, Levich plots were made for different electrolytes, Figure 3A.

Figure 3A shows the diffusion-limited current density (j_{lim}) over 300 mA cm^{-2} at the lowest rotation rate values, and then linearly decreasing with the square root of the rotation for different electrolyte mixtures between sulfuric and perchloric acids, suggesting that the kinetics is diffusion-controlled. Moreover, the negative slope (Figure 3B) can be evidence that the catalytic poison generation step is the most affected by forced convection.

As shown by spectroelectrochemical measurements,[25,26] the Au-SO_2 amount and adsorption strength both followed a tendency with the increase of electrolyte kosmotropicity and, as

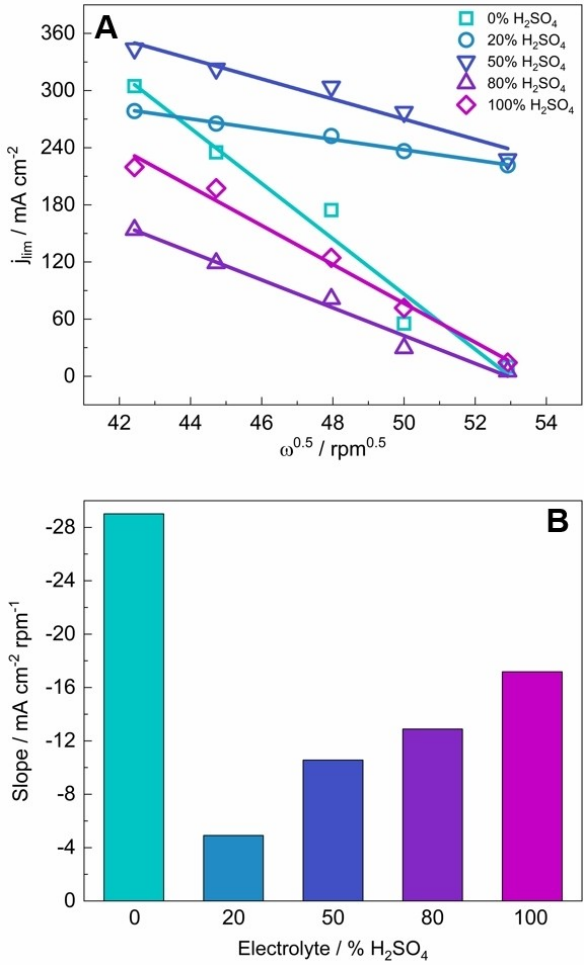

Figure 3. Levich plots obtained for SO_2OR in several compositions of electrolytes (A) and slope obtained from Figure 3A for every electrolyte composition used (B).

such, it should be expected that the slopes would follow a tendency with the increase in kosmotropicity. This is observed for the electrolytes between 20 and 100%, in which the value was getting more negative with the sulfuric acid containing (Figure 3B). In this way, it would be expected that for the 0% H_2SO_4 electrolyte (only $HClO_4$) in Figure 3B should present the lowest slope, in modulus. However, one can notice that the slope for this electrolyte is the highest. This suggests that the electrode is more susceptible to poisoning in chaotropic media and having some amount of H_2SO_4 in a $HClO_4$ solution actually suppresses the coverage process of the electrode surface. As chaotropic media is known to favor SO_2OR oscillatory reaction pathways, it can be inferred that this highly negative slope could be related to $S_2O_5^{2-}$ generation (Scheme 1).

Previous studies about mass transport influence of the SO_2OR on Au employed diluted solutions.[23,45] Samec and Weber[45] and O'Brien[23] presented a regular Levich plot for Au electrodes, as also observed for Pt,[46] graphite[47] and Pd/C[48] electrodes in non-acidic media. In all these works, the current is directly proportional to the rotation rate, explained by the Levich equation [Eq. (1)]; where j_{lim} is the diffusion-limited

current density, n the number of electrons observed in the reaction, D the diffusion coefficient, v the kinematic viscosity, C^* the electroactive species bulk concentration and ω the electrode rotation rate.

$$j_{lim} = 0.62\, n\, F\, D^{2/3}\, v^{-1/6}\, C^*\, \omega^{1/2} \quad (1)$$

While Samec and Weber[45] did not report oscillations, O'Brien observed non-linear behavior on sulfur-modified Au[23] and Pt[49] electrodes utilizing concentrated sulfuric acid solutions. The authors investigated the SO_2OR dependence on concentration of the electrolyte using the RDE, in which they showed that mass transport is highly dependent on the sulfuric acid concentration. The authors also discussed that oscillations can be observed in smaller magnitude on unmodified Au electrodes as well, but not on unmodified Pt electrodes. This was attributed to the oscillation being specific to the substrate, and not to sulfur-adsorbed layer.[23] Even though current oscillations were present, no bi-stability region was reported since the potential applied did not reach E_d, as presented in Figure 1 and in other works.[21,24–26]

O'Brien[23] also reported a decrease in D [Eq. (1)] with increasing SO_2 concentration and, most prominently, H_2SO_4 concentration. This was attributed to the strong interaction between SO_2 and SO_4^{2-} ions, which reduce the overall diffusion when the H_2SO_4 concentration increases from 0.5 to 4 mol L^{-1}. Consequently, the diffusion coefficient would decrease from 0% H_2SO_4 to 100% H_2SO_4 in the present case, and so the Levich slope would also be more negative as H_2SO_4 concentration increases. It needs to be highlighted that in the work by O'Brien[23] the solution viscosity due to the H_2SO_4 high concentration was not considered, as well as the different ion concentration between experiments. In the present case, however, the total acid concentration does not exceed 0.5 mol L^{-1}, as well as the total ion concentration, which should not interfere with the Levich slope obtained. These points must be emphasized for a clear discussion, since a conclusion about the decreasing D with higher H_2SO_4 concentration could also be suggested by interpreting Figure 3B. Nevertheless, the negative slopes obtained in Figure 3B plots forbid the direct application of Levich's model and Equation (1), but the fact that the current linearly decreases with the square root of the rotation rate is related to diffusion-limited steps in SO_2OR.[42,44,50]

An anti-Levich behavior is not unprecedented, as it is possible to find some few examples in the literature,[51–53] regarding carbon steel corrosion protection. Benchikh[52] attributed this behavior to a passivation layer growing on the electrode surface. The works presented by Tribollet's group[51,53] performed a deeper investigation in the origin of this unusual profile and attributed it to the existence of two electrode regions, one that is more insulating (passivation) and other that is more conducive and susceptible to corrosion.[53] Despite the differences in applicability, the data presented in these works have similarities with the ones presented here. The catalytic poisonous species generation can play the same role as the insulating compound and the remaining free sites are involved in charge transfer processes. Images of the electrode surface before and after electrochemical procedures are present in Figure S3. It can be noticed that initially, the electrode is uniform and presents a golden expected color (Figure S3A). After its use in SO_2OR, there is the appearance of a second surface region, circular, darker and central (Figure S3B). The electrode also presents a golden ring around the darker area, which can be related to a non-poisoned surface. This distribution can be related to an area dependent process, which is already reported for SO_2OR on carbon-based materials.[54,55]

After a longer experimental routine, the electrode still presents a golden area in the surroundings, however it is now more irregular (Figure S3C). The darker central area is then observed as reddish, which can be related to a corrosion of the electrode due to the SO_2OR. As already observed by our group,[25] ICP-MS measurements have shown that the Au electrode is corroded during the potential application, even in absence of SO_2 in the electrolyte, as also confirmed by online ICP-MS by the Mayrhofer's group.[56–58] However, such behavior is enhanced during the SO_2OR, and it is much more severe in $HClO_4$ containing electrolytes.[25] The reddish area can be related to the generation of nanosized Au particles, complexed with SO_3, as suggested in Scheme 1. This S-containing species is already reported in the literature as a stabilizing agent for Au nanoparticles.[59] In addition, in the same picture (Figure S3C) the dark material is also present, but now it is outside the metallic area of the electrode and linear flux lines can be seen.

In these works,[51,53] the authors observed a shift of the corrosion potential with rotation and related it to the anti-Levich behavior. Likewise, a similar shift can be observed in Figure 1. To sustain this analysis, electrochemical impedance spectroscopy (EIS) and Tafel analysis need to be considered. The Tafel plots are easily obtained from Figure 1, and are presented in Figures 4A and S4. For the EIS investigation, we firstly measured the open circuit potential (OCP) at each electrolyte and rotation used in this study (Table S1). After that, we applied the EIS perturbation program around the OCP. The obtained Nyquist plots are shown in Figures 4B and S5.

Tafel analysis can be influenced by mass transport,[60–62] since the reactant species concentration is normally different on the electrode surface and in the solution bulk. When the kinetically-controlled currents from Figure 4A are at least 19% of the j_{lim} in Figure 1, some significant deviation can be observed.[60,61] If the kinetic current is around 10%, the deviation is expected to be around 1.4%, as suggested by Compton's group.[61] In the present case, the mass-transport corrected and the non-corrected Tafel plots were compared (Figure S5), however, the differences in the Tafel-slope were below 0.5%, so it can be considered experimental deviation. As such, Tafel analysis were conducted without these corrections.

It can be noticed in Figure 4A that the Tafel plots shift to more negative onset potentials (E_{onset}), until a turnover at intermediate rotations (2000 rpm); then the plots are shifted to more positive E_{onset}. The slopes also drop from 55 mV at 1000 rpm to about 40 mV at 2800 rpm (all slopes are presented in Table S2). For chaotropic and kosmotropic media (Figure S4),

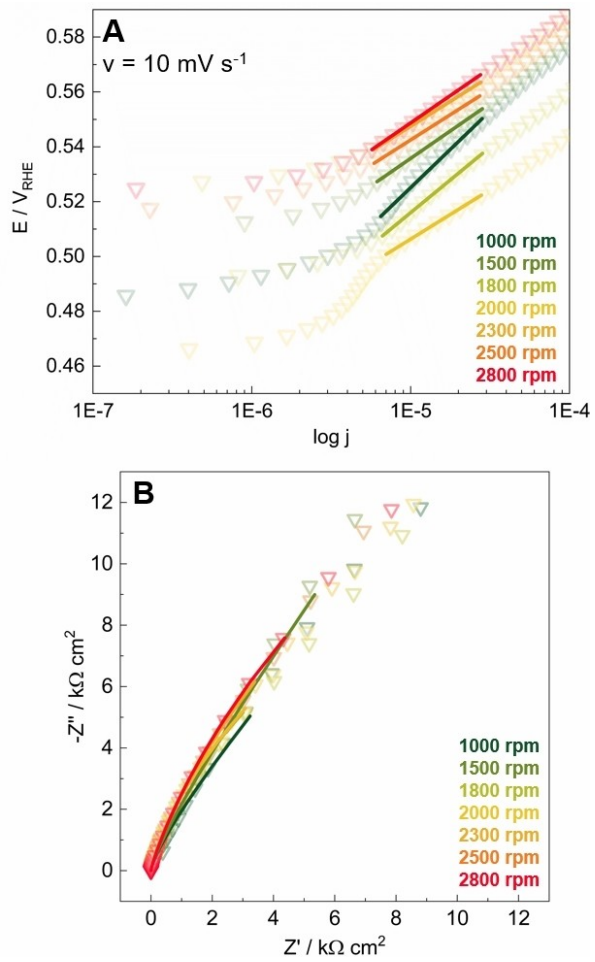

Figure 4. Tafel (A) and Nyquist (B) plots for the SO_2OR obtained at different rotation rates in a 50% H_2SO_4, $HClO_4$ electrolyte mixture. EIS measurements were performed at the OCP. Semi-transparent symbols represent the experimental data and solid lines indicate the fitting curves.

the shifts tend to more positive potentials with rotation and the slopes sharply increase.

The EIS data, Figure 4B, was fitted to the electric equivalent circuit (EEC) in Scheme 2. In there, the electrolyte resistance is represented by R_s, the double layer capacitive response by the C_{dl} and the charge transfer resistance by R_{ct}. At lower frequencies, a second time constant was also detected, which was related to a finite diffusion behavior. As the N coefficient of the CPE_{dif} increased with rotation increment, it is considered that the second time constant is related to diffusion processes.

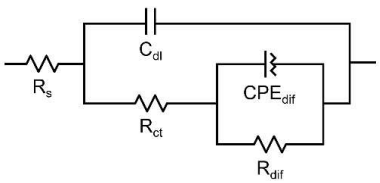

Scheme 2. EEC used to model the EIS data presented in Figure 4B and Figure S5. R_s is the electrolyte resistance, R_{ct} is the charge transfer resistance, C_{dl} is the electric double layer capacitance, R_{dif} is the diffusion resistance and CPE_{dif} is the diffusion constant phase element.

The Nyquist plots in Figure 4B show with rotation increment, the system became more resistive, with the increase of Z′, and more capacitive, with the increase of -Z″. This behavior is also seen for the $HClO_4$ electrolyte, but not for the 100% H_2SO_4 (Figure S5), where an increase in the rotation results in a decrease of the measured impedance until a turnover point at about 2000 rpm. The modeled C_{dl} and R_{ct} values are presented in Figure 5 as function of the rotation rate.

The Tafel and EIS analysis can be correlated by a Stern and Geary relationship[63] to obtain the exchange current density, Equation (2), of which b_a is the Tafel slope in V dec^{-1}, R_{ct} is the charge transfer resistance in Ω cm^2 and j_0 the current exchange current density in A cm^{-2}.

$$j_0 = b_a \,/\, 2.3\, R_{ct} \tag{2}$$

As it was also observed in the literature,[51] that C_{dl} can presented a non-monotonous variation with the rotation rate (Figure 5A). This quantity presented the same value at low rotation rates for all electrolytes, with the electrode surface coverage being roughly similar. With the rotation increment, C_{dl} increased until a maximum observed between 1500 and

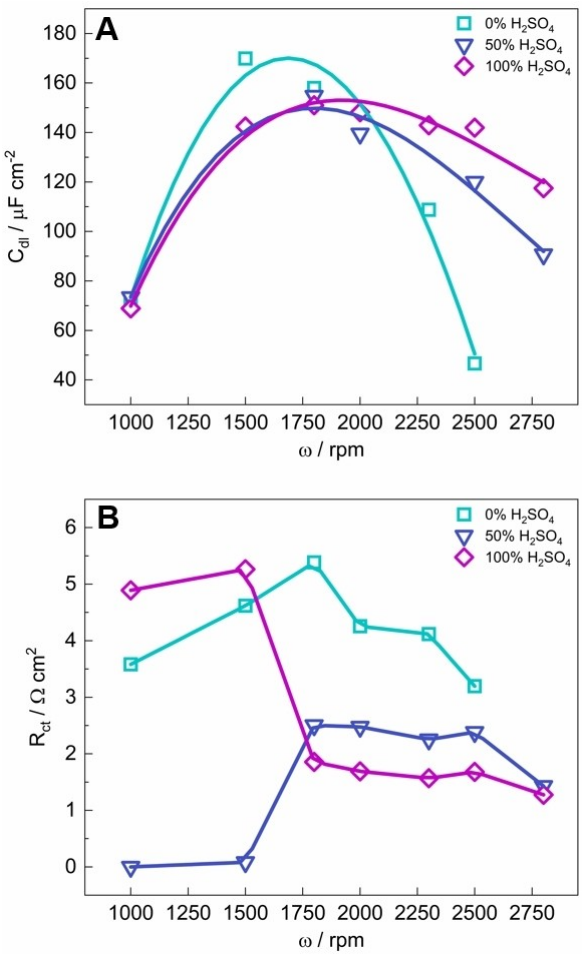

Figure 5. C_{dl} (A) and R_{ct} (B) *vs.* ω obtained from data in Figure 4B modelled by the EEC of Scheme 2. Symbols represent the experimental data and solid lines are only intended as a visual guide.

2000 rpm, and then dropped. The C_{dl} *vs.* rotation maximum shifted with the electrolyte kosmotropicity. One can also notice that the drop is inversely proportional to the H_2SO_4 content in the electrolyte, with the C_{dl} at higher rotation rates for the $HClO_4$ electrolyte presenting the lowest value, hence a freer surface.

The R_{ct} profiles observed in Figure 5B show sharp alterations in the resistance with the rotation rate. The pure H_2SO_4 and $HClO_4$ electrolytes presented a decrease in R_{ct} with the rotation, while the mixture (50%) presented an initial increase. The H_2SO_4 containing ones presented a stable R_{ct} value at high rotations which was roughly the same, around 2 $\Omega\,cm^2$. For the $HClO_4$ electrolyte this stabilization profile was not observed, since the R_{ct} linearly increases until a turnover point.

Substituting the Tafel slopes and R_{ct} values in Equation (2), it was possible to obtain the values of j_0, which are plotted *vs.* $\omega^{0.5}$ (Figure 6).

In Figure 6, j_0 presents a similar profile shape for all three electrolytes. First, j_0 increases with $\omega^{0.5}$ until reaching a given rotation, past which it is noticeable a sigmoidal or parabolic dropping pattern. Such behavior is reported, in the literature,[51] to be related to a non-uniform surface coverage, as also presented in Figure S3. Both, the slope of the linear segment and the drop at higher rotations, are of less magnitude in the pure H_2SO_4 electrolyte, while the drop in j_0 after the linear segment is most prominent in the 50% H_2SO_4:$HClO_4$ electrolyte.

The role of j_0 can be interpreted as the rate of poisonous species generation over the electrode surface,[51,53] and growth of this isolating layer is the main reason for the initial j_0 decrease. The subsequent increase should be related to the change from almost covered to full covered electrode.[51] However, the electrode was not observed to be completely covered by the isolating species, which could indicate corrosion/re-deposition of gold, which can be related to the reddish areas observed in Figure S3C.[26,51,53] The j_0 minimum was observed to be dependent on the chaotropicity as well. It was increased and shifted to higher rotations along with the H_2SO_4 containing in the electrolyte.

In this way, it was possible to show how the mass transport can influence the non-linear behavior of SO_2OR not just by the change in the mechanism at higher rotations, but also in the oscillatory behavior, since an electrolyte that presented no oscillations in static conditions,[24,25] presented galvanostatic instabilities at highly forced convection conditions. Also, the anti-Levich behavior was detected and related to the generation of two phases on the electrode surface, which can also be related to the oscillatory behavior, since these complex kinetic processes are also surface dependent.[54,55,64,65]

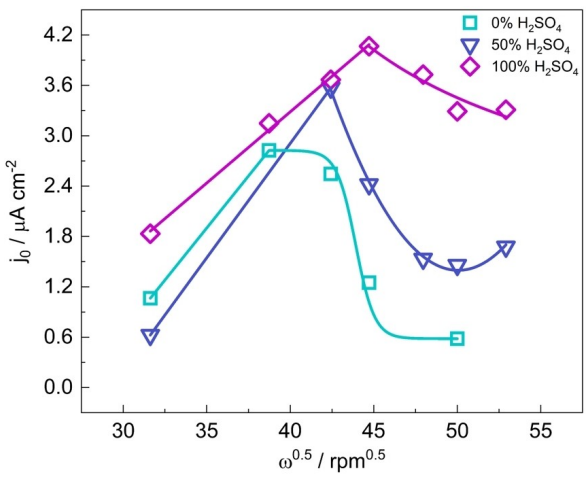

Figure 6. j_0 estimated by data in Figures 4A and 5B, plotted against $\omega^{0.5}$ for three electrolyte compositions. Symbols represent the experimental data and solid lines are only intended as a visual tendency guide.

Conclusion

The catalytic poison generation in SO_2OR on Au electrodes was observed to be enhanced by convection, causing the bi-stability region present in the *j/E* profiles to shrink with rotation increment. This behavior suggested a co-dimensional 2 cusp bifurcation; however, such phenomenon was not confirmed.

An inverted Levich behavior (anti-Levich) was present. This meant that the limiting current linearly decreased with rotation due to the formation of catalytic poison. The anti-Levich slopes were found to be highly dependent on the H_2SO_4 proportion in the electrolyte, as a very chaotropic electrolyte exhibited the highest current decrease with rotation. EIS measurements showed that the electrode-electrolyte interface changes drastically by increasing the rotation. It is believed that the formation of poisonous species could be acting as insulating layers, given that a second, dark circular region can be noticed in the center of the electrode and expanding outwards. This was corroborated by the estimation of the exchange current density, in which a sigmoidal/parabolic drop can be seen after a given rotation is achieved.

Experimental Section

A three-electrode electrochemical H-shaped cell was used, in which a frit isolates the auxiliary electrode from the working electrode and prevents SO_2 reduction to elemental sulfur, an electrochemical insulator. The electrolytes consisted of 0.50 mol L^{-1} H_2SO_4, $HClO_4$ (Sigma-Aldrich®) solutions in Milli-Q® water and mixtures between them in different proportions (0%, 20%, 50%, 80% and 100% H_2SO_4 solution, with the remaining percentage made of the $HClO_4$ solution). N_2 was bubbled for 30 min to eliminate oxygen and, for experiments containing sulfur dioxide, SO_2 (Air Liquide) was also bubbled for 30 min to ensure saturation.

The auxiliary electrode consisted in a Pt mesh and the reference electrode was the reversible hydrogen electrode (RHE), which was prepared by flame sealing a Pt wire inside a glass tube filled with the own electrolyte mixture being used in the given electrochemical procedure.

The working electrode was a Au rotating disk electrode (RDE, d = 4 mm) in hanging meniscus configuration.[66,67] The Au electrode was firstly polished with Alumina suspensions with decreasingly diameter size (1, 0.3 and 0.05 μm) for about two minutes each, posteriorly submitted to chemical cleaning, which consisted in

sonicating the electrode in different solvents following an increment in polarity (toluene, acetone, ethanol – all LabSynth® – and water, two times in this last one) for about two minutes each. Then, the electrode was submitted to electrochemical polishing in a 0.50 mol L^{-1} H_2SO_4 solution, which consisted in cyclic voltammetry in the range of −0.5 to 1.6 V_{RHE}, at a sweep rate of 10 mV s^{-1}, for 10 cycles. The electrochemical surface area (ECSA) of the Au electrode was determined by Cu underpotential deposition using 0.50 mol L^{-1} $CuSO_4$ (dissolved from LabSynth® 98% w/w $CuSO_4 \cdot 5H_2O$) in a 0.50 mol L^{-1} H_2SO_4 solution, in agreement with methods proposed in the literature.[68] The average ECSA was found to be about 0.03 cm^2, however, each independent electrochemical procedure was corrected by the ECSA measured before-hand to avoid any deviations in the current density calculated between experiments.

To perform hydrodynamic procedures, the rotation rate of the Au RDE was controlled by a Pine AFMSRCE and potential/galvano perturbations were carried out by an Autolab PGSTAT302N bipotentiostat (perturbation programs are inserted in the figures). For impedance measurements, the working electrode was kept at the OCP until its stabilization (about half an hour) and this value suffered sinusoidal disturbance with amplitude of 10 mV and frequencies varying from 10^5 to 10^{-2} Hz. All procedures were performed at room temperature (25 °C).

Acknowledgements

The authors would like to thank Fundação de Amparo à Pesquisa do Estado de São Paulo (FAPESP) for the financial support (grants #2015/26308-7 and #2020/15230-5). A. H. B. D. and L. D. A. would also like to thank FAPESP for their grants (#2013/25592-8, #2018/13944-0, #2021/08007-0 and #2021/09630-3). We also thankfully acknowledge the support of the RCGI – Research Centre for Greenhouse Gas Innovation, hosted by the University of S˜ao Paulo (USP) and sponsored by FAPESP and Shell Brasil, and the strategic importance of the support given by ANP (Brazil's National Oil, Natural Gas, and Biofuels Agency) through the R&D levy regulation.

Conflict of Interest

The authors declare no conflict of interest.

Data Availability Statement

The data that support the findings of this study are available from the corresponding author upon reasonable request.

Keywords: Electrochemistry · Mass transport · Reaction mechanisms · Sulfur dioxide · Water splitting

[1] M. Li, X. Zhang, G. Li, *Energy* **2016**, *94*, 693–704.
[2] V. F. McNeill, *Trends Chem.* **2019**, *1*, 5–8.
[3] P. Nikolaidis, A. Poullikkas, *Renewable Sustainable Energy Rev.* **2017**, *67*, 597–611.
[4] S. Sgouridis, M. Carbajales-Dale, D. Csala, M. Chiesa, U. Bardi, *Nat. Energy* **2019**, *4*, 456–465.
[5] S. W. Sheehan, E. R. Cave, K. P. Kuhl, N. Flanders, A. L. Smeigh, D. T. Co, *Chem.* **2017**, *3*, 3–7.
[6] D. D. Wagman, J. E. Kilpatrick, W. J. Taylor, K. S. Pitzer, F. D. Rossini, *J. Res. Natl. Bur. Stand (1934)* **1945**, *34*, 143.
[7] T. da Silva Veras, T. S. Mozer, D. da Costa Rubim Messeder dos Santos, A. da Silva César, *Int. J. Hydrogen Energy* **2017**, *42*, 2018–2033.
[8] L. S. José, *Sustainable Hydrogen Production Processes: Energy, Economic and Ecological Issues*, Springer International Publishing, **2017**.
[9] S. Singh, S. Jain, V. Ps, A. K. Tiwari, M. R. Nouni, J. K. Pandey, S. Goel, *Renewable Sustainable Energy Rev.* **2015**, *51*, 623–633.
[10] I. Katsounaros, S. Cherevko, A. R. Zeradjanin, K. J. J. Mayrhofer, *Angew. Chem. Int. Ed.* **2014**, *53*, 102–121; *Angew. Chem.* **2014**, *126*, 104–124.
[11] I. Godwin, A. Rovetta, M. Lyons, J. Coleman, *Curr. Opin. Electrochem.* **2018**, *7*, 31–35.
[12] M. E. G. Lyons, R. L. Doyle, M. P. Browne, I. J. Godwin, A. A. S. Rovetta, *Curr. Opin. Electrochem.* **2017**, *1*, 40–45.
[13] T. A. Matias, A. L. A. Parussulo, P. A. Benavides, R. R. Guimarães, A. H. B. Dourado, M. Nakamura, S. I. C. de Torresi, M. Bertotti, K. Araki, *Electrochim. Acta* **2018**, *283*, 18–26.
[14] H. Ju, S. Giddey, S. P. S. Badwal, *Electrochim. Acta* **2017**, *229*, 39–47.
[15] S. Díaz-Abad, M. Millán, M. A. Rodrigo, J. Lobato, *Catalysts* **2019**, *9*, 63.
[16] J. A. Staser, J. W. Weidner, *J. Electrochem. Soc.* **2009**, *156*, B16.
[17] Z. Klimont, S. J. Smith, J. Cofala, *Environmental Research Letters* **2013**, *8*, 014003.
[18] R. J. Kriek, J. P. van Ravenswaay, M. Potgieter, A. Calitz, V. Lates, M. E. Björketun, S. Siahrostami, J. Rossmeisl, *J. South Afr. Inst. Min. Metall* **2013**, *113*, 593–604.
[19] R. J. Kriek, J. Rossmeisl, S. Siahrostami, M. E. Björketun, *Phys. Chem. Chem. Phys.* **2014**, *16*, 9572–9579.
[20] C. Quijada, F. J. Huerta, E. Morallón, J. L. Vázquez, L. E. A. Berlouis, *Electrochim. Acta* **2000**, *45*, 1847–1862.
[21] C. Quijada, *Electrochim. Acta* **2001**, *46*, 651–659.
[22] J. A. O'Brien, J. T. Hinkley, S. W. Donne, *J. Electrochem. Soc.* **2010**, *157*, F111.
[23] J. A. O'Brien, J. T. Hinkley, S. W. Donne, *J. Electrochem. Soc.* **2012**, *159*, F585–F593.
[24] A. H. B. Dourado, R. L. Munhos, H. Varela, S. I. Córdoba de Torresi, M. Arenz, *J. Phys. Chem. C* **2018**, *122*, 1243–1247.
[25] A. H. B. Dourado, R. L. Munhos, N. A. Silva, V. del Colle, G. G. A. Carvalho, P. v. Oliveira, M. Arenz, H. Varela, S. I. Córdoba de Torresi, *ACS Catal.* **2019**, *9*, 8136–8143.
[26] A. H. B. Dourado, N. A. Silva, R. L. Munhos, V. del Colle, M. Arenz, H. Varela, S. I. Córdoba de Torresi, *ChemElectroChem.* **2020**, *7*, 1843–1850.
[27] W. Kunz, J. Henle, B. W. Ninham, *Curr. Opin. Colloid Interface Sci.* **2004**, *9*, 19–37.
[28] B. C. Gibb, *Nat. Chem.* **2019**, *11*, 963–965.
[29] A. G. Zelinsky, *Electrochim. Acta* **2016**, *188*, 727–733.
[30] C. Quijada, J. L. Vázquez, *Recent Res. Dev. Electrochem.* **2000**, *3*, 137–181.
[31] P. Strasser, M. Eiswirth, M. T. M. Koper, *J. Electroanal. Chem.* **1999**, *478*, 50–66.
[32] M. T. M. Koper, in *Adv Chem. Phys* (Ed.: S. A. Rice), John Wiley & Sons, Inc., Hoboken, NJ, USA, **2007**, pp. 161–298.
[33] J. L. Hudson, T. T. Tsotsis, *Chem. Eng. Sci.* **1994**, *49*, 1493–1572.
[34] M. T. M. Koper, *J. Chem. Soc. Faraday Trans.* **1998**, *94*, 1369–1378.
[35] M. T. M. Koper, *Electrochim. Acta* **1992**, *37*, 1771–1778.
[36] S. H. Strogatz, *Choice Reviews Online* **1994**, *32*, 32–0994-32-0994.
[37] F. Xu, *Zeitschrift für Phys. Chemie* **1990**, *166*, 79–91.
[38] L. S. Marcoux, R. N. Adams, S. W. Feldberg, *J. Phys. Chem.* **1969**, *73*, 2611–2614.
[39] S. Karp, L. Meites, *J. Electroanal. Chem. Interfacial Electrochem.* **1968**, *17*, 253–265.
[40] S. Karp, *J. Phys. Chem.* **1968**, *72*, 1082–1082.
[41] P. A. Malachesky, L. S. Marcoux, R. N. Adams, *J. Phys. Chem.* **1966**, *70*, 4068–4070.
[42] Z. Galus, C. Olson, H. Y. Lee, R. N. Adams, *Anal. Chem.* **1962**, *34*, 164–166.
[43] R. Vargas, C. Borrás, J. Mostany, B. R. Scharifker, *Electrochim. Acta* **2012**, *80*, 326–333.
[44] D. Pletcher, R. Greff, R. Peat, L. M. Peter, J. Robinson, in *Instrumental Methods in Electrochemistry*, Elsevier, West Sussex, **2010**, pp. 113–148.
[45] Z. Samec, J. Weber, *Electrochim. Acta* **1975**, *20*, 413–419.
[46] E. Skavås, T. Hemmingsen, *Electrochim. Acta* **2007**, *52*, 3510–3517.
[47] T. Hunger, F. Lapicque, *Electrochim. Acta* **1991**, *36*, 1073–1082.
[48] R. A. Márquez-Montes, R. E. Orozco-Mena, D. Lardizábal-Gutiérrez, D. Chávez-Flores, A. López-Ortíz, V. H. Ramos-Sánchez, *Electrochem. Commun.* **2019**, *104*, DOI 10.1016/j.elecom.2019.106481.

[49] J. A. O'Brien, J. T. Hinkley, S. W. Donne, *Electrochim. Acta* **2011**, *56*, 4224–4230.
[50] J. Masa, C. Batchelor-McAuley, W. Schuhmann, R. G. Compton, *Nano Res.* **2014**, *7*, 71–78.
[51] N. Srisuwan, N. Ochoa, N. Pébère, B. Tribollet, *Corros. Sci.* **2008**, *50*, 1245–1250.
[52] A. Benchikh, R. Aitout, L. Makhloufi, L. Benhaddad, B. Saidani, *Desalination* **2009**, *249*, 466–474.
[53] N. Ochoa, F. Moran, N. Pébère, B. Tribollet, *Corros. Sci.* **2005**, *47*, 593–604.
[54] M. Dao, J. Wang, *J. Electroanal. Chem.* **2020**, *877*, 114472.
[55] T. Hunger, F. Lapicque, *Electrochim. Acta* **1991**, *36*, 1073–1082.
[56] S. Cherevko, A. A. Topalov, A. R. Zeradjanin, I. Katsounaros, K. J. J. Mayrhofer, *RSC Adv.* **2013**, *3*, 16516.
[57] S. Cherevko, A. R. Zeradjanin, A. A. Topalov, G. P. Keeley, K. J. J. Mayrhofer, *J. Electrochem. Soc.* **2014**, *161*, 501–507.
[58] O. Kasian, S. Geiger, K. J. J. Mayrhofer, S. Cherevko, *The Chemical Record* **2019**, *19*, 2130–2142.
[59] R. N. P. Colombo, D. F. S. Petri, S. I. Córdoba de Torresi, V. R. Gonçales, *Electrochim. Acta* **2015**, *158*, 187–195.
[60] D. Li, C. Lin, C. Batchelor-McAuley, L. Chen, R. G. Compton, *J. Electroanal. Chem.* **2018**, *826*, 117–124.
[61] C. Batchelor-McAuley, D. Li, R. G. Compton, *ChemElectroChem.* **2020**, *7*, 3844–3851.
[62] R. M. Torresi, O. R. Cámara, C. P. de Pauli, M. C. Giordano, *Electrochim. Acta* **1987**, *32*, 1291–1301.
[63] M. Stern, A. L. Geary, *J. Electrochem. Soc.* **1957**, *104*, 56.
[64] I. Z. Kiss, Z. Kazsu, V. Gáspár, *Phys. Chem. Chem. Phys.* **2009**, *11*, 7669.
[65] Y. Wang, J. L. Hudson, *AIChE J.* **1991**, *37*, 1833–1843.
[66] H. M. Villullas, M. L. Teijelo, *J. Electroanal. Chem.* **1995**, *384*, 25–30.
[67] H. M. Villullas, M. L. Teijelo, *J. Electroanal. Chem.* **1995**, *385*, 39–44.
[68] S. R. Brankovic, J. X. Wang, R. R. Adžić, *Surf. Sci.* **2001**, *474*, L173–L179.

Manuscript received: October 11, 2022
Revised manuscript received: December 14, 2022

RESEARCH ARTICLE

Mass transport effects: The use of fossil fuels led to the production of unwanted chemicals, such as sulfur dioxide, which could be oxidized to sulfuric acid while facilitating hydrogen generation. This reaction presents a complex mechanism dependent of convection and electrolyte chaotropicity, being attributed to the reaction pathway alteration and generation of catalytic poison.

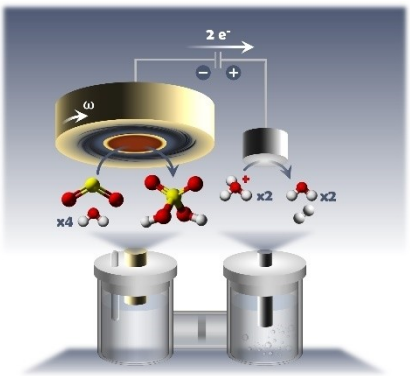

*L. D. De Angelis, Prof. Dr. S. I. Córdoba de Torresi, Dr. A. H. B. Dourado**